



HAL
open science

Birefringent optical retarders from laser 3D-printed dielectric metasurfaces

Simonas Varapnickas, Samlan Chandran Thodika, Fabien Moroté, Saulius Juodkazis, Mangirdas Malinauskas, Etienne Brasselet

► **To cite this version:**

Simonas Varapnickas, Samlan Chandran Thodika, Fabien Moroté, Saulius Juodkazis, Mangirdas Malinauskas, et al.. Birefringent optical retarders from laser 3D-printed dielectric metasurfaces. Applied Physics Letters, 2021, 118 (15), pp.151104. 10.1063/5.0046978 . hal-03260856

HAL Id: hal-03260856

<https://hal.science/hal-03260856>

Submitted on 4 Jul 2021

HAL is a multi-disciplinary open access archive for the deposit and dissemination of scientific research documents, whether they are published or not. The documents may come from teaching and research institutions in France or abroad, or from public or private research centers.

L'archive ouverte pluridisciplinaire **HAL**, est destinée au dépôt et à la diffusion de documents scientifiques de niveau recherche, publiés ou non, émanant des établissements d'enseignement et de recherche français ou étrangers, des laboratoires publics ou privés.

Birefringent optical retarders from laser 3D-printed dielectric metasurfaces

Cite as: Appl. Phys. Lett. **118**, 151104 (2021); doi: [10.1063/5.0046978](https://doi.org/10.1063/5.0046978)

Submitted: 9 February 2021 · Accepted: 30 March 2021 ·

Published Online: 16 April 2021 · Publisher error corrected: 20 April 2021







View Online



Export Citation



CrossMark

Simonas Varapnickas,¹ Samlan Chandran Thodika,² Fabien Moroté,²  Saulius Juodkazis,³ 
Mangirdas Malinauskas,^{1,a)}  and Etienne Brasselet^{2,a)} 

AFFILIATIONS

¹Physics Faculty, Laser Research Center, Vilnius University, Sauletekio Ave. 10, Vilnius Lt-10223, Lithuania

²University Bordeaux, CNRS, LOMA, UMR 5798, Talence, France

³Optical Sciences Center and ARC Training Centre in Surface Engineering for Advanced Materials (SEAM), Faculty of Science, Engineering and Technology, Swinburne University of Technology, Hawthorn VIC 3122, Australia

^{a)}Authors to whom correspondence should be addressed: mangirdas.malinauskas@ff.vu.lt and etienne.brasselet@u-bordeaux.fr

ABSTRACT

Structuring light attracts continuous research effort due to its impactful applications in optical information and communications, laser material processing, optical imaging, or optical manipulation of matter. In particular, femtosecond laser direct writing of photoresists is a technology dedicated to the creation of optically isotropic free-form 3D micro-optical elements with size, spatial resolution, and surface quality that qualify to demanding integrated optics needs. Here, we report on the design, production, and characterization of dielectric metasurface birefringent optical retarders made from femtosecond laser 3D printing technology whose polarization conversion efficiency is more than 10 times larger than that previously reported Wang *et al.*, Appl. Phys. Lett. **110**, 181101 (2017)]. As the flexibility of the fabrication process allows considering arbitrary orientation of the artificially engineered optical axis, these results open up for 3D printed geometric phase optical elements.

Published under license by AIP Publishing. <https://doi.org/10.1063/5.0046978>

Since a few decades, different kinds of pixelated spatial light modulators have been a primary choice for preparing light field properties with tailored intensity, phase, and polarization spatial profiles. The dominant character of these technologies lies in the ability to reconfigure the shaping of light by individual electrical control of nowadays $\sim 10^6$ (liquid crystal devices) up to $\sim 10^7$ (digital micromirror devices) constitutive elementary units having a typical individual footprint of about $100 \mu\text{m}^2$.¹ Such multi-purpose optical elements with an active area of $\sim 1 \text{ cm}^2$, however, come with bulky packaging and are, thus, restricted so far to table-top installations. In parallel, shaping light down to subwavelength resolution over macroscopic areas has become accessible owing to nanofabrication technologies such as electron beam lithography, ion beam milling, or atomic layer deposition. This eventually led to ultrathin two-dimensional (2D) optical elements—metasurfaces—that can arbitrarily process light properties over wavelength-thick subwavelength-structured materials and that are expected to seed wave-based industrial applications.² Still, achieving reconfigurable and tunable metasurfaces remains an open and challenging issue both at technical and fundamental levels. A step in this direction has been made by exploiting artificially engineered optical

anisotropy, which allows imparting polarization-controlled optical functions to metasurfaces. Specifically, the spin-orbit optical interactions for photons³ have been unveiled as a core ingredient whose extension to three-dimensions (3D) remains to be developed.⁴ In contrast, creating optically isotropic 3D micro/nanostructures using tightly focused ultrafast lasers has been under study for a long time since early studies on glasses and polymers.^{5,6} Nowadays, femtosecond laser direct writing of photoresists is routinely used to 3D print free-form scalar dielectric permittivity distributions, not only in research labs but also in emerging high-tech companies, seeding future markets in optics and photonics.^{7,8} All this provides with a handful of tools to address the following challenge: making laser 3D printing technology capable of creating free-form optics endowed with structured tensorial dielectric properties and, hence, with polarization-controlled optical functions.

Preliminary effort has been reported recently using space-variant gratings laser printed out of dielectric photoresists.⁹ The resulting structures, characterized by a uniform birefringent phase retardation Δ , have been shown to act as geometric phase optical elements, although exhibiting a poor polarization conversion purity η up to a

couple of percent at best. Recalling that 100% purity, which corresponds to $\Delta = \pi$ modulo 2π in the absence of absorption,⁹ is formally required to fully exploit the spin-orbit features of geometric phase optical elements,³ which appears as a crippling practical drawback. In order to tackle with the latter state-of-the-art limitations, here we deal with transmission gratings whose spatial period Λ is small enough to suppress all the diffraction orders other than the zeroth-order one. This condition, which is not satisfied in Ref. 9, allows dealing with a proper effective uniaxial medium. Namely, considering a relief grating at the interface between two dielectric media—here, the photopolymerized resist and the air, see Fig. 1(a)—this corresponds to $\Lambda < \lambda/n$,¹⁰ where λ is the operating wavelength in vacuum and n the corresponding refractive index of the material.

We choose the popular hybrid photo-resist SZ2080TM known for its low shrinkage and high optical transmissivity, without the addition of photo-initiator. Laser printing is achieved by using a custom-built femtosecond-laser direct writing setup consisting of frequency-doubled mode-locked laser Pharos (Light Conversion Ltd.) delivering optical pulses at a wavelength of 515 nm with a duration of 300 fs at a repetition rate of 200 kHz and linear nanopositioning stages (Aerotech Inc.) synchronized with a galvanometric scanner for beam steering through the 4F correlator and oil-immersion objective lens (Carl Zeiss AG, 63 \times , NA = 1.4). We refer to Ref. 11 for a detailed description of the setup, while the description of pre-bake and development protocols might be found in Ref. 12. With the aim of producing subwavelength gratings, as small as possible grating period Λ is desirable; however, laser printing resolution gives a lower bound. We select $\Lambda = 750$ nm, which ensures robust fabrication, and we choose a filling factor $F = 0.5$, which gives almost maximal birefringence while minimizing the structure aspect ratio for a given grating height [see the inset of Fig. 1(b)]. Accounting for the material dispersion, this implies to work in the near infrared domain, $\lambda \approx 1080$ nm. Equipment constraints lead us to carry out the optical characterization at a wavelength of $\lambda = 1050$ nm, for which the complex refractive index is estimated as $n + ik \approx 1.45(1 + i/100)$ from Ref. 13 while $n \approx 1.50$ is found from Ref. 20. The expected artificial birefringence is evaluated from the second-order effective medium approach,¹⁴ discarding material

absorption. Namely, choosing the case study of a rectangular waveform subwavelength grating illuminated at normal incidence, one approximately gets an effective uniaxial medium whose refractive indices along a direction parallel (\parallel) and perpendicular (\perp) to the grating wavevector are given by

$$n_{\parallel} = n_{\parallel,0} \left[1 + \frac{\pi^2 \Lambda^2}{3\lambda^2} F^2 \bar{F}^2 n_{\parallel,0}^4 n_{\perp,0}^2 \left(1 - \frac{1}{n^2} \right)^2 \right]^{1/2}, \quad (1)$$

$$n_{\perp} = n_{\perp,0} \left[1 + \frac{\pi^2 \Lambda^2}{3\lambda^2} F^2 \bar{F}^2 \frac{1}{n_{\perp,0}^2} (n^2 - 1)^2 \right]^{1/2}, \quad (2)$$

where λ is the wavelength, $\bar{F} = 1 - F$, $n_{\perp,0} = (n^2 F + \bar{F})^{1/2}$, and $n_{\parallel,0} = n(F + n^2 \bar{F})^{-1/2}$. The calculated birefringence $dn = n_{\parallel} - n_{\perp}$ is shown in Fig. 1(b) where the first-order evaluation $dn_0 = n_{\parallel,0} - n_{\perp,0}$ is shown as well. One gets $dn = -0.085$ ($n = 1.45$) and $dn = -0.103$ ($n = 1.50$) for $F = 0.5$, which tells us that a grating height $h^{(\pi)} = 6.2 \mu\text{m}$ ($n = 1.45$) and $h^{(\pi)} = 5.1 \mu\text{m}$ ($n = 1.50$) is required to reach the above-mentioned half-wave retardance criterion. The corresponding fabrication aspect ratio $2h^{(\pi)}/\Lambda = 16.5$ ($n = 1.45$) and $2h^{(\pi)}/\Lambda = 13.6$ ($n = 1.50$) is too high to produce with present state-of-the-art and brings a fabrication limitation, which also explains the poor purity values obtained so far.⁹ This issue is solved by taking advantage of the free form capabilities of 3D laser printing, designing a multilayer structures. The idea is to stack several gratings lying at both ends of N disks (except for the bottom one standing on the BK7 glass substrate) with a thickness of $H = 10 \mu\text{m}$ and a diameter of $100 \mu\text{m}$ that are piled up and suspended by side pillars [see Fig. 1(c)]. This allows adding up the effects of $2N - 1$ individual gratings with subwavelength thickness h , each of them, therefore, being actually a metasurface. The possible fabrication of space-variant birefringent structures has also been explored as shown in Fig. 1(d). However, we restrict the present study to homogeneous retarders as the fabrication challenges prevent us to obtain satisfying ensuing vortex beam shaping so far.

Birefringent optical retarders are 3D-printed on BK7 coverslips drop-coated with the photoresist. The supporting structures (disks and pillars) are printed at constant parameters optimized to ensure

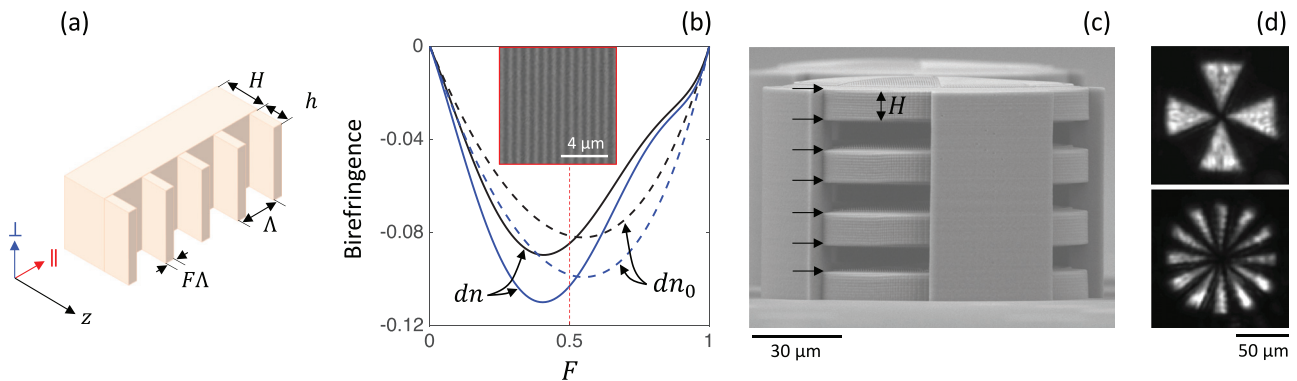


FIG. 1. (a) Sketch of the rectangular waveform grating and definition of the geometrical parameters. (b) Dependence of the first-order (dn_0) and second-order (dn) artificial birefringence as a function of the filling factor for $\lambda = 1050$ nm and $\Lambda = 750$ nm, with $n = 1.45$ (black curves) and $n = 1.50$ (blue curves). Inset: top-view scanning electron microscope (SEM) image of a grating with $\Lambda = 750$ nm and $h \sim 500$ nm. (c) Side-view SEM image of a multilayer structure made of $N = 4$ stacked disks and 8-sector space-variant grating design, suspended by four side parallelepiped pillars (a second structure is seen in the back). The arrows indicate the location of the $2N - 1$ grating layers of a space-variant grating structure. (d) Images of 8-segment and 24-segment space-variant metaretarders with $N = 6$ observed between crossed linear polarizers at 1050 nm.

efficient yet stable and highly repeatable production, i.e., a pulse energy of 0.8 nJ and a spatial overlap of 75% (interpulse distance of 50 nm), hatching was 250 nm, and slicing 500 nm. About 8 μm gaps were left between each two stacked disks allowing adequate circulation of solvent during structure development. For the gratings, we use a constant writing velocity that maintains a pulse spatial overlap of ~99.9% and we fabricate nine kinds of them by using three distinct pulse energies E_i and three different distances between the centers of the voxels defining the grating and that defining the first layer of the pad on which sits the grating. Choosing a few distinct writing conditions allows us to explore an extended set of optical performances. At a given parameter, fabrication takes from 8 min for $N = 1$ to 72 min for $N = 6$. Note that, for a given structure, all the grating layers are fabricated under identical laser writing conditions for $N > 1$.

On the one hand, the structural parameters of the fabricated micro-optical elements are characterized using an atomic force microscope (AFM) and illustrated in Fig. 2, with only the grating at the top of the structure being analyzed. We studied 23 structures in total spanning $1 \leq N \leq 3$ and various laser writing parameters. The grating period is estimated from AFM profilometry over 12 periods, and the grating depth is estimated from the height histogram collected from a $15 \mu\text{m} \times 7.5 \mu\text{m}$ area as shown in Fig. 2(a) [see Figs. 2(b) and 2(c), respectively]. On the other hand, the optical performance of the meta-retarders is carried out by measuring the power fraction of the output beam whose polarization state is orthogonal to that of the incident

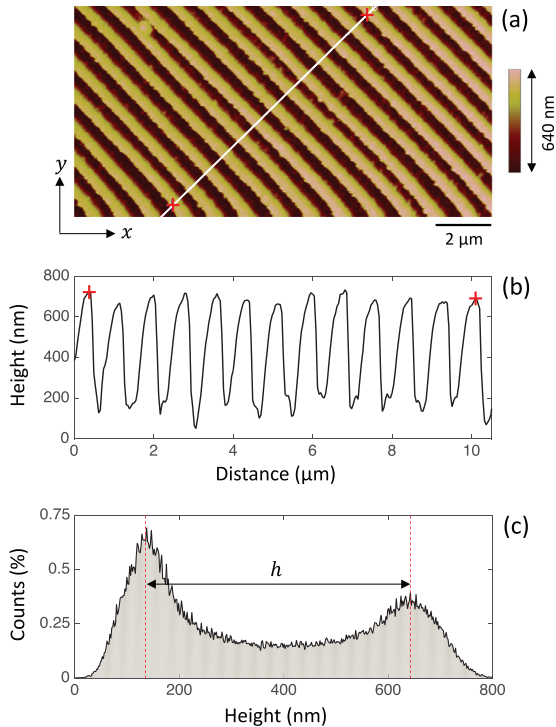


FIG. 2. Typical AFM structural characterization of a 3D laser printed uniform grating. (a) AFM image of a $15 \mu\text{m} \times 7.5 \mu\text{m}$ area. The crosses and white line refer to the height cross section shown in panel (b). (c) Statistics of the height over the image shown in panel (a), from which the grating height h is measured.

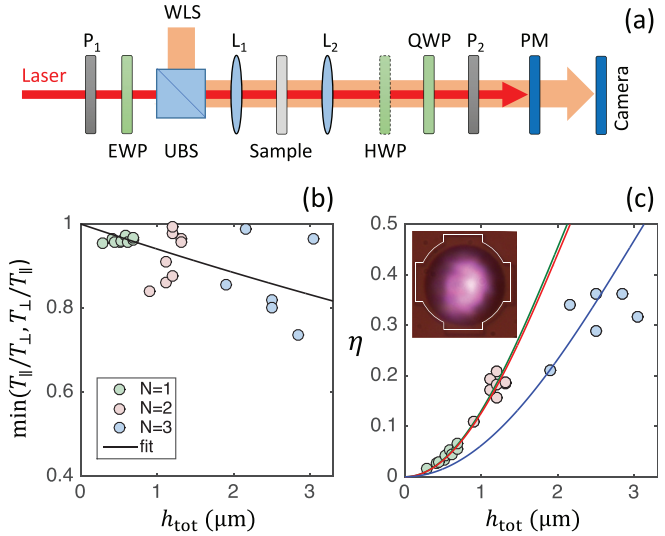


FIG. 3. (a) Experimental setup used to measure the purity parameter η . $P_{1,2}$: polarizers; EWP: electrically tunable liquid crystal retarder, used to prepare a circular polarization state impinging on the sample, accounting from residual polarization modifications of the beam splitter; BS: beam splitter; WLS: white light source (for structure imaging); L_1 : 50 mm focal length lens; L_2 : $4\times$ microscope objective lens with a numerical aperture of $\text{NA} = 0.1$; HWP: half-wave retarder (placed or removed in order to select the handedness of the circular polarization projection of the output beam); QWP: quarter-wave retarder; PM: power meter. (b) Ratio of power transmittances for an incident linear polarization state parallel and perpendicular to the grating wavevector, which gives access to the parameter α_a . (c). Purity η as a function of the total grating height h_{tot} for a set of 23 structures with $1 \leq N \leq 3$. The curves refer to the adjustment of the experimental data with the formula given by Eq. (3) (see the text for details). Inset: image of the laser beam ($\lambda = 1050 \text{ nm}$) spot in the plane of the sample, whose contour is marked by a thin line to facilitate its observation.

beam. The measurements are performed using a circularly polarized incident paraxial beam with a diameter of $\sim 50 \mu\text{m}$ and gives access to η , see Fig. 3, where the offset value $\eta_0 = 0.047$ measured without the sample is subtracted from the data. In this figure, we assume that h does not depend on the $2N - 1$ grating layers for a given structure and we introduce the total height $h_{\text{tot}} = (2N - 1)h$. An effective description of the stacked structure is, thus, made by considering it as a single grating with height h_{tot} , for which the purity parameter is expressed as¹⁵

$$\eta(h_{\text{tot}}) = \frac{1}{2[1 + \delta^2(h_{\text{tot}})]} \left\{ [1 - \delta(h_{\text{tot}})]^2 \cos^2 \left[\frac{\Delta(h_{\text{tot}})}{2} \right] + [1 + \delta(h_{\text{tot}})]^2 \sin^2 \left[\frac{\Delta(h_{\text{tot}})}{2} \right] \right\}, \quad (3)$$

where $\Delta(h_{\text{tot}}) = 2\pi dn h_{\text{tot}}/\lambda$ is the effective birefringent phase retardation of the structure and $\delta(h_{\text{tot}}) = \exp(-\alpha_a h_{\text{tot}})$, with $\alpha_a > 0$, its effective anisotropic on-axis amplitude transmission loss coefficient that could result from the combined effects of uncontrolled nanostructured material inhomogeneities and multiple reflections. The coefficient α_a is experimentally assessed from the ratio of on-axis transmitted power for a linearly polarized incident beam with orientation perpendicular and parallel to the grating wavevector, $\min(T_{\perp}/T_{\parallel}, T_{\parallel}/T_{\perp}) = \exp(-2\alpha_a h_{\text{tot}})$ [see Fig. 3(b)], which gives

$\alpha_a = 0.031 \mu\text{m}^{-1}$. Then, adjusting the dataset for η with Eq. (3) gives access to $|dn|$, which is done for structures with $N=1$ only (green solid curve), $N=1$ and $N=2$ only (red solid curve), and all of them (blue solid curve) [see Fig. 3(c)]. This gives $|dn| = 0.124$, $|dn| = 0.122$, and $|dn| = 0.083$, respectively. Discarding the anisotropic losses leaves the results virtually unchanged, and $N=3$ appears detrimental to the effective birefringent performances.

Although we use an effective model ignoring the multiple reflections at the various interfaces and the fact that the fabricated grating waveform departs from rectangular profiles, the obtained value for the artificial birefringence does not depart much from our crude estimate. This validates a decent macroscopic understanding of the obtained optical performances. Nevertheless, the variability of the available data for the refractive index $n^{13,20}$ calls for *in situ* quantitative measurements of the refractive properties of the polymerized material towards reliable design. We notice that the obtained polarization conversion performance is up to 10 times larger than that previously reported,⁹ which makes the 3D laser printing approach a realistic pathway to create dielectric geometric phase optical metasurfaces in the visible and infrared domains.

The transmittance is another relevant parameter to assess the quality of geometric phase optical elements, and the benefits of a multilayer approach come with some drawbacks as the number of interfaces increases with N , so does the transmittance. Experimentally, the latter is measured from the ratio of the power transmitted through the structure to that transmitted through the glass substrate. A preliminary experiment is made with a set of structures *without gratings* for $N=1$ to 4, see Fig. 4(a), with $T_{w/o}$ denoting the corresponding transmittance. Neglecting the multiple reflections between various interfaces, the measurements are compared with the expression derived from the Fresnel transmittances of individual interfaces. Namely,

$$T_{w/o} = T_{g,p} T_{a,p}^{2N-1} / T_{a,g}, \quad (4)$$

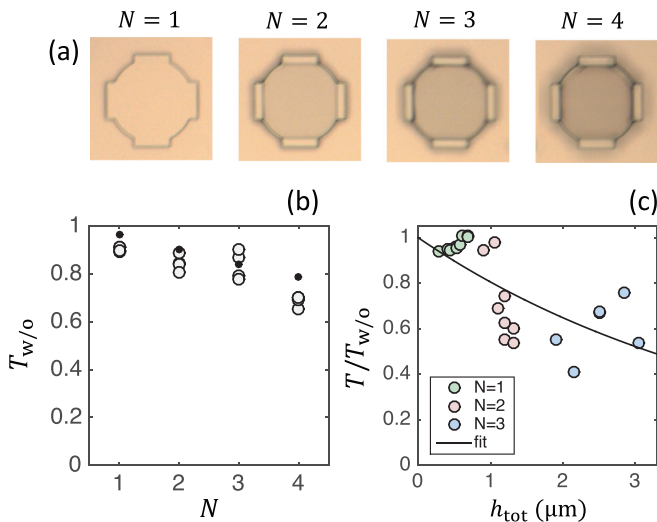


FIG. 4. (a) Bright field natural light image of structures without gratings for $1 \leq N \leq 4$. (b) Transmittance of the structures as those shown in panel (a). The data correspond to 4 distinct structures for each N . (c) Transmittance associated with the grating layers themselves (see the text for details) for a set of 23 structures with $1 \leq N \leq 3$. The solid line refers to the adjustment of the experimental data with the formula given by Eq. (5).

where (g, p, a) stand for (glass, photoresist, air) and $T_{1,2} = 4n_1n_2 / (n_1 + n_2)^2$ refers to the transmittance through the interface between media 1 and 2 having the refractive indices n_1 and n_2 , respectively. The results are shown in Fig. 4(b), where we use $n_g = 1.52$ and $n_a = 1$, and a fair description is obtained. Then, we measure the transmittance T of the 23 previous structures *with gratings* for $N=1-3$. This allows extracting the mean attenuation coefficient per unit length $\bar{\alpha}$ of the gratings themselves from the relationship

$$T/T_{w/o} = \exp(-\bar{\alpha}h_{tot}), \quad (5)$$

which gives $\bar{\alpha} = 0.217 \mu\text{m}^{-1}$. This means that the search for higher overall birefringent phase retardation by means of ever-increasing stacking eventually compromises the viability of the device. Nevertheless, we recall that the subwavelength criterion is only marginally satisfied, and the use of larger wavelength or smaller grating period provides ways to solve such limitations. Increasing the spatial regularity of the grating and increasing its height are other routes for improvements. Interestingly, combining the present approach with recent developments about scalable 3D sintering techniques based on heat treatment,¹⁶ both refractive index increase and downsizing of the initially printed structures can be expected. All these options go in favor of reaching larger efficiencies of the optical element, ηT , and give a roadmap for future works for which telecom wavelengths (1310 nm and 1550 nm) should retain specific attention for applications.

In summary, these results broaden the range of academic and industrial impacts of an ever-improving robust laser additive manufacturing technology.¹⁷⁻¹⁹ In particular, the inherent 3D structuring capabilities of the proposed approach allow considering the fabrication of dielectric devices on curved and flexible substrates, while the structured material itself can be reconfigurable under external forcing, for instance, by using elastomers. Noteworthy, antireflection coating strategies toward enhanced efficiencies are not doomed to suffer from 3D complexity recalling that topography-independent approaches exist, such as atomic layer deposition of titanium or zirconium oxides. More generally, these results foster further development of laser additive manufacturing technology where both scalar and anisotropic part of the dielectric permittivity tensor will be treated as independent degrees of freedom in 3D and for which future fundamental and application prospects are yet to come.

We acknowledge the financial support from EU Horizon 2020, Research and Innovation programme LASERLAB-EUROPE JRA Project No. 871124 (S.V. and M.M.), from the Initiative of Excellence of the University of Bordeaux program, grant agreement ANR-10-IDEX-03-02 (S.J. and E.B.), and from the H2020-MSCA-IF-2018 Programme, Grant No. 838199 (S.C.T.).

DATA AVAILABILITY

The data that support the findings of this study are available from the corresponding author upon reasonable request.

REFERENCES

- H. Yu, J. Park, K. Lee, J. Yoon, K. Kim, S. Lee, and Y. Park, "Recent advances in wavefront shaping techniques for biomedical applications," *Curr. Appl. Phys.* **15**, 632–641 (2015).
- J. Scheuer, "Optical metasurfaces are coming of age: Short-and long-term opportunities for commercial applications," *ACS Photonics* **7**, 1323–1354 (2020).

- ³K. Y. Bliokh, F. J. Rodríguez-Fortuño, F. Nori, and A. V. Zayats, "Spin-orbit interactions of light," *Nat. Photonics* **9**, 796 (2015).
- ⁴F. Cardano and L. Marrucci, "Spin-orbit photonics," *Nat. Photonics* **9**, 776–778 (2015).
- ⁵K. M. Davis, K. Miura, N. Sugimoto, and K. Hirao, "Writing waveguides in glass with a femtosecond laser," *Opt. Lett.* **21**, 1729–1731 (1996).
- ⁶S. Maruo, O. Nakamura, and S. Kawata, "Three-dimensional microfabrication with two-photon-absorbed photopolymerization," *Opt. Lett.* **22**, 132–134 (1997).
- ⁷S. Thiele, C. Pruss, A. Herkommer, and H. Giessen, "3d printed stacked diffractive microlenses," *Opt. Lett.* **27**, 35621–35630 (2019).
- ⁸A. Butkute, L. Cekanavicius, G. Rimselis, D. Gailevicius, V. Mizeikis, A. Melninkaitis, T. Baldacchini, L. Jonusauskas, and M. Malinauskas, "Optical damage thresholds of microstructures made by laser three-dimensional nanolithography," *Opt. Lett.* **45**, 13–16 (2020).
- ⁹X. Wang, A. Kuchmizhak, E. Brasselet, and S. Juodkazis, "Dielectric geometric phase optical elements fabricated by femtosecond direct laser writing in photoresists," *Appl. Phys. Lett.* **110**, 181101 (2017).
- ¹⁰W. Stork, N. Streibl, H. Haidner, and P. Kipfer, "Artificial distributed-index media fabricated by zero-order gratings," *Opt. Lett.* **16**, 1921–1923 (1991).
- ¹¹P. Danilevičius, S. Rekštytė, E. Balčiūnas, A. Kraniauskas, R. Širmenis, D. Baltriukienė, V. Bukelskienė, R. Gadonas, V. Sirvydis, A. Piskarskas, and M. Malinauskas, "Laser 3D micro/nanofabrication of polymers for tissue engineering applications," *Opt. Laser Technol.* **45**, 518–524 (2013).
- ¹²B. Sanchez-Padilla, A. Žukauskas, A. Aleksanyan, A. Balčytis, M. Malinauskas, S. Juodkazis, and E. Brasselet, "Wrinkled axicons: Shaping light from cusps," *Opt. Express* **24**, 24075–24082 (2016).
- ¹³A. Žukauskas, G. Batavičiūtė, M. Ščiuka, Z. Balevičius, A. Melninkaitis, and M. Malinauskas, "Effect of the photoinitiator presence and exposure conditions on laser-induced damage threshold of ormosil (sz2080)," *Opt. Mat.* **39**, 224–231 (2015).
- ¹⁴S. Rytov, "Electromagnetic properties of a finely stratified medium," *Zh. Eksp. Teor. Fiz.* **29**, 605–616 (1956) [*Sov. Phys. JETP* **2**, 466–475 (1956)].
- ¹⁵E. Brasselet, "Optical angular momentum conversion in a nanoslit: Comment," *Opt. Lett.* **38**, 3890–3890 (2013).
- ¹⁶D. Gailevicius, V. Padolskytė, L. Mikoliūnaitė, S. Šakirzanovas, S. Juodkazis, and M. Malinauskas, "Additive-manufacturing of 3. Glass-ceramics down to nanoscale resolution," *Nanoscale Horiz.* **4**, 647–651 (2019).
- ¹⁷K. Weber, F. Hütt, S. Thiele, T. Gissibl, A. Herkommer, and H. Giessen, "Single mode fiber based delivery of oam light by 3D direct laser writing," *Opt. Express* **25**, 19672–19679 (2017).
- ¹⁸A. Bertoncini and C. Liberale, "3D printed waveguides based on photonic crystal fiber designs for complex fiber-end photonic devices," *Optica* **7**, 1487–1494 (2020).
- ¹⁹J. Li, S. Thiele, B. C. Quirk, R. W. Kirk, J. W. Verjans, E. Akers, C. A. Bursill, S. J. Nicholls, A. M. Herkommer, H. Giessen *et al.*, "Ultrathin monolithic 3D printed optical coherence tomography endoscopy for preclinical and clinical use," *Light Sci. Appl.* **9**, 1–10 (2020).
- ²⁰V. Melissinaki, O. Tsilipakos, M. Kafesaki, M. Farsari, and S. Pissadakakis, "Micro-ring resonator devices prototyped on optical fiber tapers by multi-photon lithography," *IEEE J. Select. Top. Quantum Electron.* **27**, 1–7 (2021).